Journal of Power Sources 202 (2012) 269–275

Contents lists available at SciVerse ScienceDirect

Journal of Power Sources

journal homepage: www.elsevier.com/locate/jpowsour

Investigation of $CrSi_2$ and $MoSi_2$ as anode materials for lithium-ion batteries

Fabrice M. Courtel, Dominique Duguay, Yaser Abu-Lebdeh*, Isobel J. Davidson

National Research Council Canada, 1200 Montreal Road, Ottawa, Ontario K1A 0R6, Canada

ARTICLE INFO

Article history:
Received 7 October 2011
Received in revised form
14 November 2011
Accepted 15 November 2011
Available online 25 November 2011

Keywords:
$CrSi_2$
$MoSi_2$
Silicide
Li-ion batteries
Anode material

ABSTRACT

We report on the suitability of the two metal silicides $MoSi_2$ and $CrSi_2$ as anode materials for Li-ion batteries. The two materials were synthesized by high energy ball milling of the corresponding metals and X-ray diffraction was used to follow the evolution/formation of the crystalline phases. The in-house prepared powders have shown better battery performance than commercial powders (as-received or ball-milled). We observed that 20 h were necessary for the formation of $MoSi_2$ whereas 100 h were needed for the formation of the $CrSi_2$ powder. The best battery performance was obtained with the synthesized $CrSi_2$ powder that has a theoretical capacity value of 469 mAh g^{-1}. This powder provided capacities of 340, 262, 167, 110, and 58 mAh g^{-1} at C/12, C/6, C/2, C, and 2C, respectively. Cycling at 60 °C showed higher capacity values, but with a faster fade of these values.

1. Introduction

Most commercial lithium-ion batteries use graphitic carbon as the anode material due to its low cost, long cycle life, and very stable capacity [1]. However, the reversible electrochemical intercalation of lithium ions in its structure leads to the intercalation of one lithium per six carbons (LiC_6) that results in capacities theoretically limited to only 372 mAh g^{-1}. Silicon has been studied for quite a while as anode material. Silicon is abundant, quite inexpensive, non-toxic, and provides a very high theoretical capacity over 3500 mAh g^{-1} ($Si + 3.75\ Li^+ + 3.75\ e^- \leftrightarrow SiLi_{3.75}$) [2]. However it suffers from large structural volume changes during charge/discharge cycling of the battery reaching 300–400% [1,3,4]. This gives rise to mechanical stresses that lead to cracks and eventual disintegration of the electrode and a failure of the battery [5]. Intermetallic compounds, such as silicides M–Si (with M: Mg [6–8], Mn [2,9], Mo [10], Fe [9,11], Ni [12], Nb, Ta, V, Ca, Cr [13,14], and Ti) [1] were first reported by Anani and Huggins as anode materials for Li-ion batteries [14], especially Mg_2Si [6] and $CrSi_2$ [14]. Since, more work have been performed on silicon and silicon-metal alloys; on this regard, two interesting reviews have recently been published on the subject by Park et al. [15] and Larcher et al. [2]. The in situ formation of the inactive metal compound acts as a matrix that mitigates the volume change. Mg_2Si has an anti-fluorine structure that was shown to accommodate Li-insertion according to the following path: $Mg_2Si + 2Li + 2e \rightarrow Li_2MgSi + Mg$, followed by reaction of Mg with lithium to form an MgLi alloy [14,16]. However, other groups reported the following reaction pathway [7,8]: $Mg_2Si + 3Li + 3e \rightarrow 2MgLi + SiLi$. Initial capacities are typically usually high but the reversible capacity is quite low. It has also been reported that lithium could be inserted into the structure of $CrSi_2$, but is limited by slow kinetics at room temperature [17]. Nevertheless, using a composite of $CrSi_2$ and lithium, Weydanz et al. reported initial discharge capacities ranging from 650 to 800 mAh g^{-1}, depending on the Li:$CrSi_2$ ratio used [17].

We decided to investigate the battery performance of pristine $CrSi_2$ (without lithium additive) at room temperature (R.T.) and at 60 °C. We also report on the battery behavior of its twin compound $MoSi_2$ as a comparison [10]. These two pristine silicides have never been investigated as anode materials for Li-ion batteries. Based on Anani and Huggins work [14] we estimated theoretical capacities of 804 mAh g^{-1} for $MoSi_2$ and 580 mAh g^{-1} for $CrSi_2$. These values are in the range of capacities expected for future anode materials in cathode-limited batteries as calculated by Appleby et al. [4].

Herein we report the investigation of synthesized and commercially available $CrSi_2$ and $MoSi_2$. The powders were tested as received and also ball-milled via high energy ball-milling (HEBM) at different times. In addition, a comparison with synthesized $CrSi_2$ and $MoSi_2$ powders prepared by HEBM was also performed. Lithium batteries (half-cells) were assembled with the different materials and tested galvanostatically at different rates and by cyclic voltammetry.

* Corresponding author. Tel.: +1 613 949 4184; fax: +1 613 990 0347.
E-mail address: Yaser.Abu-Lebdeh@nrc-cnrc.gc.ca (Y. Abu-Lebdeh).

0378-7753/$ – see front matter.
doi:10.1016/j.jpowsour.2011.11.047

2. Experimental

2.1. Materials

Chromium silicide ($CrSi_2$, 230 mesh, 99+%), molybdenum (Mo, 1–2 μm, >99.9%), and silicon (Si, 325 mesh, 99%) were purchased from Sigma–Aldrich. Molybdenum silicide ($MoSi_2$, 99.5%) and chromium (Cr, <10 μm, 99.8%) were purchased from Alfa Aesar. Carbon graphite E-KS4 and Super S carbon were purchased from Lonza G+T (Switzerland) and Timcal (Switzerland), respectively. Sodium carboxymethyl cellulose (NaCMC, viscosity 42.0 mPa s) was purchased from Calbiochem and used as a 5 wt% solution dissolved in double distilled H_2O. Sodium carboxymethyl cellulose (NaCMC) was used as a binder in this work instead of conventional PVDF due to its superior performance with silicon-based anode materials.

2.2. Synthesis

$CrSi_2$ and $MoSi_2$ powders were first used as received and then ball-milled for 20 h using HEBM technique. A 50 mL tungsten carbide vial (8004, Spex) and three tungsten carbide beads (10.75 g each, Spex) were used along with a powder/ball ratio of 1/3.2. $CrSi_2$ and $MoSi_2$ were also synthesized via the same HEBM technique using the same powder/ball ratio. The synthesis was performed using Mo, Cr and Si powders as starting materials mixed in a M/Si atomic ratio of 1/2. The mixture was ball-milled until the right phase was obtained, which took 100 h for $CrSi_2$ and 20 h for $MoSi_2$. HEBM was performed using a SPEX8000 ball miller, and the vials were sealed under argon atmosphere before milling.

2.3. Characterization

Powder X-ray diffraction was carried out using a Bruker AXS D8 diffractometer with a Cu Kα source with a step size of 0.03° and an acquisition time of 1 s per step. The patterns were analyzed by the Rietveld refinement method [18] using the software TOPAS 4 from Bruker AXS [19]. The crystallite sizes were determined using the fundamental parameter approach method developed by Cheary et al. [20]. Powders were also characterized by scanning electron microscopy (SEM) using a JEOL 840 A. Battery cycling was carried out on half-cells using 2325-type coin cells assembled in an argon-filled glove box. Capacity measurements were performed by galvanostatic experiments carried out on a multichannel Arbin battery cycler. The working electrode was first charged (lithiated) down to 5 mV versus Li/Li^+ at different C-rates and then discharged (delithiated) up to 2 V versus Li/Li^+. The values of the cell parameters, the crystallite sizes, and the composition percentages are given with an error value between brackets.

The working electrodes were prepared as follows: the active material was mixed with 5 wt% Super S carbon, 5 wt% Graphite and 10 wt% binder. The electrode films were made by spreading onto a high purity copper foil current collector (cleaned using a 2.5% HCl solution in order to remove the copper oxide layer) using an automated doctor-blade and then dried overnight at 85 °C in a convection oven. Individual disk electrodes (Ø = 12.5 mm) were punched out, dried at 80 °C under vacuum overnight and then pressed under a pressure of 0.5 metric ton. Electrodes were made of 3–4 mg of active material. A lithium metal disk (Ø = 16.5 mm) was used as a negative electrode (counter electrode and reference electrode). 70 μL of a solution of 1 M $LiPF_6$ in ethylene carbonate/dimethyl carbonate (EC:DMC, 1:1, v/v) was used as electrolyte and spread over a double layer of microporous propylene separators (Celgard 3501, thickness = 30 μm, Ø = 2.1 mm). The cells were assembled in an argon-filled dry glove box at room temperature.

3. Results and discussion

3.1. X-ray diffraction

XRD has been performed on the $MoSi_2$ and $CrSi_2$ commercial powders, as-received and ball-milled in order to follow the decrease of the crystallite sizes. X-ray patterns were also recorded during the HEBM steps of the Mo–Si and Cr–Si mixtures.

Fig. 1 shows the XRD profiles of commercial $MoSi_2$ as a function of HEBM time. Using the Rietveld refinement method, the composition (in wt%) of the as-received commercial $MoSi_2$ powder was of: 93.3(1)% $MoSi_2$, 4.9(1)% Mo_5Si_3, and 0.8(6)% Mo. The $MoSi_2$ phase exhibits a tetragonal *I4/mmm* structure with cell parameter of: $a = 3.20508(3)$ Å and $c = 7.84638(9)$ Å, and a crystallite size of 306(14) nm was calculated. The secondary tetragonal *I4/mcm* Mo_5Si_3 phase has cell parameters of $a = 9.6462(6)$ Å and $c = 4.9064(5)$ Å and crystallite sizes of 210(100) nm. After 20 h of HEBM a decrease of $MoSi_2$ content and an increase of the Mo_5Si_3 phase have been observed. The powder is then composed of 70.7(1)% $MoSi_2$, 28.1(1)% Mo_5Si_3, and 1.2(4)% Mo. As expected, a decrease in the crystallite sizes to 173(10) nm for $MoSi_2$ and 5(2) nm for Mo_5Si_3 has been observed. Fig. 2 shows the X-ray patterns of the Mo–Si mixture HEBM from 0 h to 20 h. Before the HEBM started, as expected, a mixture of elemental molybdenum and silicon was observed. After only 3 h of HEBM, the tetragonal $MoSi_2$ phase started appearing along with the disappearance of the Si peaks and the decrease of the Mo peak intensity, as observed by Ma et al. [10]. After 20 h of HEBM, the in-house prepared powder is composed of 93.2% $MoSi_2$ (two different crystalline structures) and 6.8% Mo. The first $MoSi_2$ identified phase is the tetragonal *I4/mmm* structure that represents 71.4%, with cell parameters of: $a = 3.2032(2)$ Å and $c = 7.8658(7)$ Å, and crystallite sizes of 13(18) nm. The second identified $MoSi_2$ structure has a *P6222* space group, represents 21.8% and has cell parameters of: $a = 4.704(6)$ Å and $c = 6.094(4)$ Å, and crystallite sizes of 10(8) nm. Smaller crystallite sizes are observed for the in-house synthesized $MoSi_2$ compared to the commercial HEBM $MoSi_2$ powder.

Fig. 3 shows the XRD profiles of commercial $CrSi_2$ as a function of ball-milling time. By Rietveld refinement, the calculated composition of the as-received commercial $CrSi_2$ powder was 99.75% $CrSi_2$ and 0.25% CrSi. The $CrSi_2$ phase exhibits a *P6422* structure with cell parameters of: $a = 4.42784(5)$ Å and $c = 6.3726(1)$ Å, and using the fundamental parameter approach method crystallite sizes of 187(63) nm were calculated. After 20 h of HEBM, the $CrSi_2$ crystallite size has decreased to 7(1) nm with cell parameters of $a = 4.4284(5)$ Å and $c = 6.380(2)$ Å; the two secondary phases, CrSi and Si were no longer visible. The in-house prepared $CrSi_2$ powder took a longer time to prepare than the $MoSi_2$ powder. The phase started appearing after 20 h of HEBM, along with the disappearance of the chromium phase. After 100 h of HEBM, the chromium phase is at a minimum level. The powder is then composed of 65.1% $CrSi_2$, 27.2% Cr_5Si_3, and 7.7% Cr. The $CrSi_2$ powder showed small crystallite size of 9(3) nm, similarly for the Cr_5Si_3 powder at 9(4) nm Fig. 4.

3.2. Scanning electron microscopy

Fig. 5 shows the SEM micrographs of the three $CrSi_2$ powders and three $MoSi_2$ powders. As shown in Fig. 5a and c, the as-received commercial $CrSi_2$ and $MoSi_2$ show smooth particles ranging from 5 to 10 μm in size. After 20 h of HEBM, a decrease in the particle size was noticed for both powders. As shown by Fig. 5b and d sizes now range at and below 5 μm. $CrSi_2$ powder made by 100 h of HEBM directly from a Cr–Si mixture shows a small and an homogeneous size distribution, around 2 μm with aggregate sizes up to

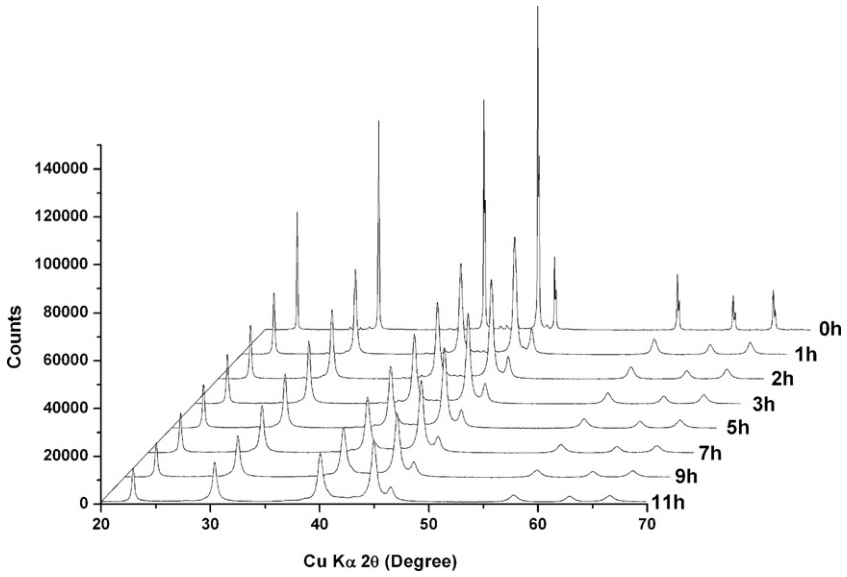

Fig. 1. XRD patterns of commercial $MoSi_2$ during the HEBM steps.

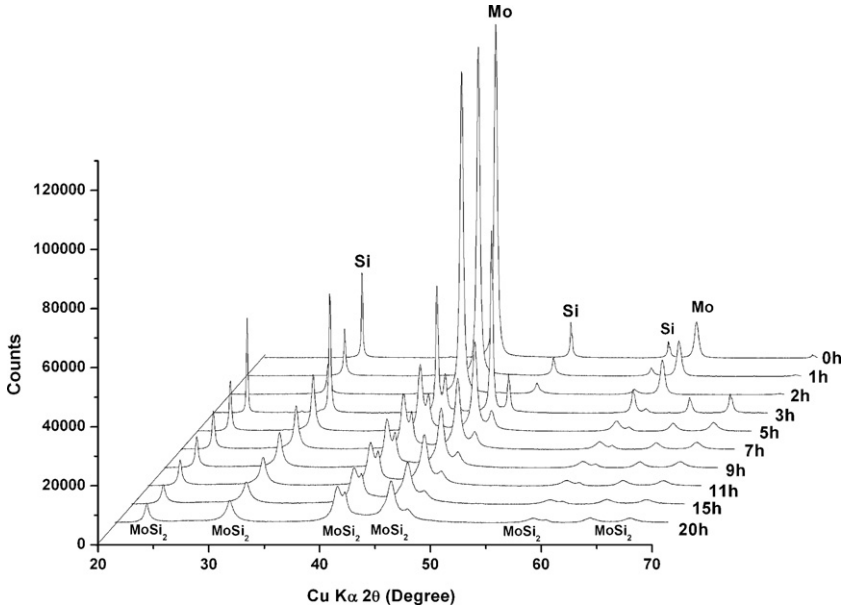

Fig. 2. XRD patterns of the Mo–Si mixture during the HEBM steps.

6–7 μm. The $MoSi_2$ powder prepared the same way with 20 h of HEBM shows particle sizes around 1 μm.

3.3. Battery cycling

All six powders have been tested as anode materials in half-cells using lithium metal as a counter and reference electrode. The C-rate and theoretical capacities were calculated using the work performed by Anani and Huggins [14] who estimated the lithium storage capacities of several silicides, including molybdenum and chromium silicides. Capacity values of the different molybdenum and chromium silicides indentified by XRD have been calculated using the formula reported in reference [21]: Cap. ($mAh\,g^{-1}$) = (96,500 × number of Li^+ exchanged)/(molecular weight of the silicide × 3.6). The capacity values, ranging from 279 to 804 $mAh\,g^{-1}$, are summarized in Table 1.

The theoretical capacity values of the six investigated powders have been calculated according to the composition obtained via the Rietveld refinement method applied to the XRD patterns. The capacity values summarized in Table 2 do not take into account a possible amorphous silicon phase that was not detectable by XRD.

Fig. 6 shows the performance and the rate capability of commercial $MoSi_2$, as-received and HEBM for 20 h, and in-house made $MoSi_2$ electrodes. After 20 cycles at C/12, the previously mentioned powders showed capacities of 100, 115 and 135 $mAh\,g^{-1}$,

Table 1
Theoretical capacity values of the different molybdenum and chromium silicides.

Silicide	$MoSi_2$	Mo_5Si_3	$CrSi_2$	CrSi	Cr_5Si_3
Lithium stored [14]	4.56	5.88	2.34	0.93	4.32
Capacity ($mAh\,g^{-1}$)	804	279	580	311	336

Table 2
Composition and theoretical capacity values of commercial (as-received and HEBM) and in-house synthesized molybdenum and chromium silicides.

Silicide	$MoSi_2$ commercial as-received	$MoSi_2$ commercial 20 h HEBM	$MoSi_2$ in-house 20 h HEBM	$CrSi_2$ commercial as-received	$CrSi_2$ commercial 20 h HEBM	$CrSi_2$ in-house 100 h HEBM
Composition from Rietveld refinement (wt%)	93.3 $MoSi_2$	70.7 $MoSi_2$	93.2 $MoSi_2$	99.75 $CrSi_2$	93.53 $CrSi_2$	65.1 $CrSi_2$
	4.9 Mo_5Si_3	28.1 NMo_5Si_3 Mo	6.8 Mo	0.25 CrSi 1.2Mo	6.47Cr	Cr_5Si_3 7.7Cr
Capacity ($mAh\,g^{-1}$)	764	647	749	579	542	469

respectively, which is lower than graphite (330 $mAh\,g^{-1}$ at C/12). According to Huggins, the expected capacities are 764, 647, and 749 $mAh\,g^{-1}$, respectively. The lower capacities could not be attributed to poor electronic conductivity as it is reported that $MoSi_2$ is a good electrical conductor of 3.5×10^4 $S\,cm^{-1}$ [22,23] but most probably to poor ionic conductivity as it is also possible that the lithium diffusion coefficient is very low at R.T. Another possibility is that $MoSi_2$ might not be very reactive towards lithium, as pointed out by Dahn et al. for most silicides [9]. Fig. 6 also reports the rate capability of these three electrodes, that are obviously also very low. However the powder made in-house provided the best capacity values.

In order to improve the lithium mobility in $MoSi_2$, a half-cell made of the in-house prepared powder has been cycled at 60 °C. It showed a high first discharge capacity of 450 $mAh\,g^{-1}$ and an irreversible capacity of 235 $mAh\,g^{-1}$, which represents about 65% of the first discharge capacity. After 20 cycles, the electrode has a capacity of only 75 $mAh\,g^{-1}$. As reported by Fleischauer et al., the capacity fade for silicon-rich silicides could be related to the increased degree of $Li_{15}Si_4$ crystallization at higher temperature as

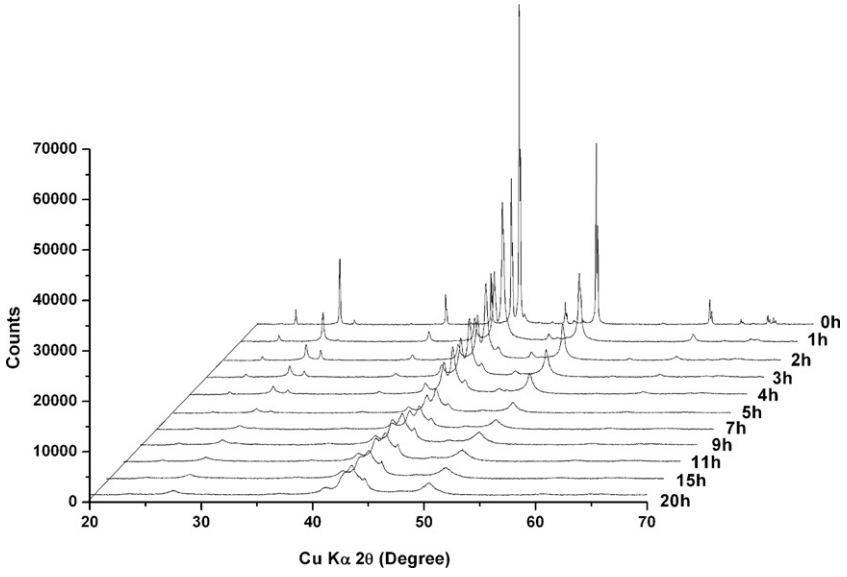

Fig. 3. XRD patterns of commercial $CrSi_2$ during the HEBM steps.

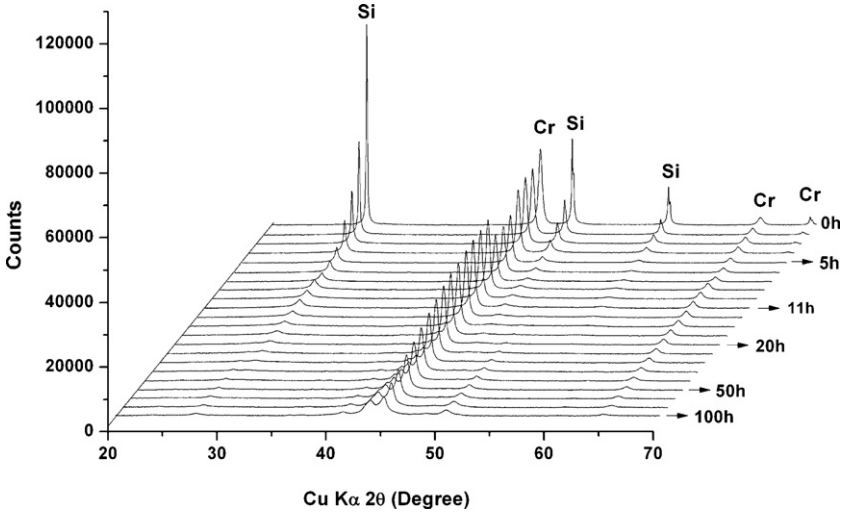

Fig. 4. XRD patterns of the Cr–Si mixture during the HEBM steps.

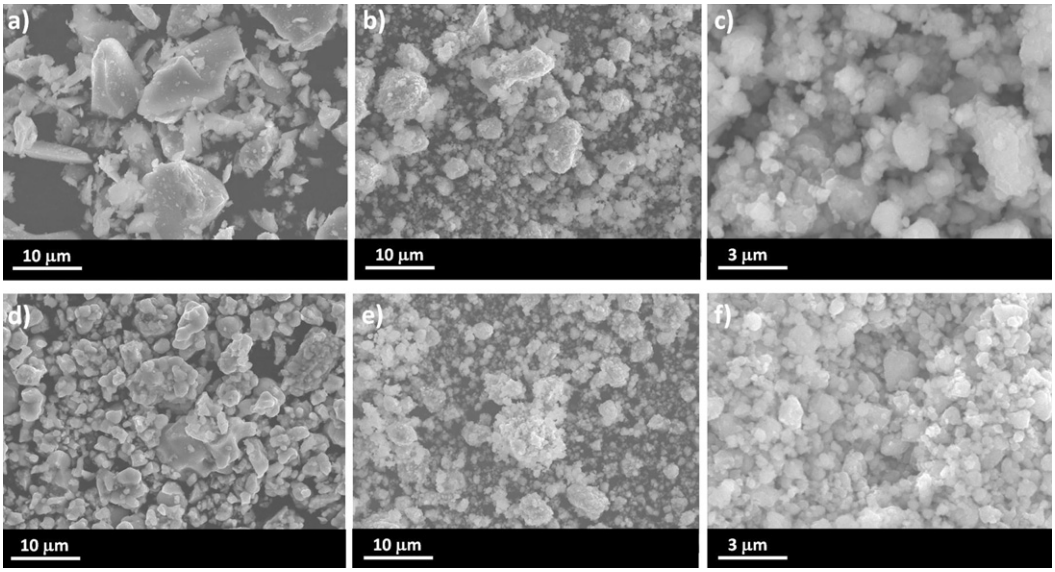

Fig. 5. SEM micrographs of (a) as-received commercial $CrSi_2$, (b) commercial $CrSi_2$ after 20 h of HEBM, (c) synthesized $CrSi_2$, (d) as-received commercial $MoSi_2$, (e) commercial $MoSi_2$ after 20 h of HEBM, and (f) synthesized $MoSi_2$.

opposed to amorphous $Li_{15}Si_4$ which is more reactive [24]. It could also be due to the degradation of the electrolyte and the formation of a thicker SEI layer at the surface of the particles. Fig. 7 shows the voltage profile of the $MoSi_2$ powder prepared in-house by 20 h of HEBM. It shows a discharge that starts most probably with the formation of a SEI at about 1.25 V. An insertion plateau is also observed at low potential at about 0.01 V. The delithiation started with a short plateau at 0.2 V, and then a slope (straight line) between 0.005 V and 2 V. According to Anani and Huggins, the addition of molybdenum to the binary silicon–lithium system produces three additional phases in the ternary phase diagram Mo–Si–Li: $MoSi_2$, Mo_5Si_3, and Mo_3Si. As a consequence, it gives rise to two additional equilibria: $MoSi_2$–Mo_5Si_3–$SiLi_{3.25}$ and Mo_5Si_3–Mo_3Si–$SiLi_{4.4}$ [14]. It is important to point out that molybdenum does not form an alloy with lithium. The reactions corresponding to these equilibria are shown by Eqs. (1) and (2):

$$20MoSi_2 + 91Li^+ + 91e^- \leftrightarrow 4Mo_5Si_3 + 28SiLi_{3.25} \quad (1)$$

$$15Mo_5Si_3 + 88Li^+ + 88e^- \leftrightarrow 25Mo_3Si + 20SiLi_{4.4} \quad (2)$$

Chromium is in the same group as molybdenum in the periodic table and shares some physical and chemical properties, and its silicide compounds are of similar interest. Similar to $MoSi_2$, the performance of pristine $CrSi_2$ has never been reported in the literature, only Weydanz et al. reported first discharge capacities of a composite of $CrSi_2$ and lithium which varied from 650 to 800 mAh g^{-1} as a function of the Li:$CrSi_2$ ratio used [17]. Fig. 8 shows the performance of different $CrSi_2$ electrode materials: the as-received and 20 h ball-milled commercial powders and the in-house synthesized powders. The as-received powder provides a very low capacity, around 75 mAh g^{-1}. The HEBM (20 h) powder showed enhancement in capacity with a first discharge of 330 mAh g^{-1}, which represents 61% of the theoretical capacity and an irreversible capacity between the first and the second cycle of about 50 mAh g^{-1} (15% of the first discharge capacity). This powder showed a reversible capacity of 225 mAh g^{-1} after 20 cycles at C/12.

The in-house prepared $CrSi_2$ powder showed better performance than the commercial one. When cycled at room temperature, a reversible capacity of 340 mAh g^{-1} was obtained for this powder after 20 cycles at C/12, which is almost as good as the

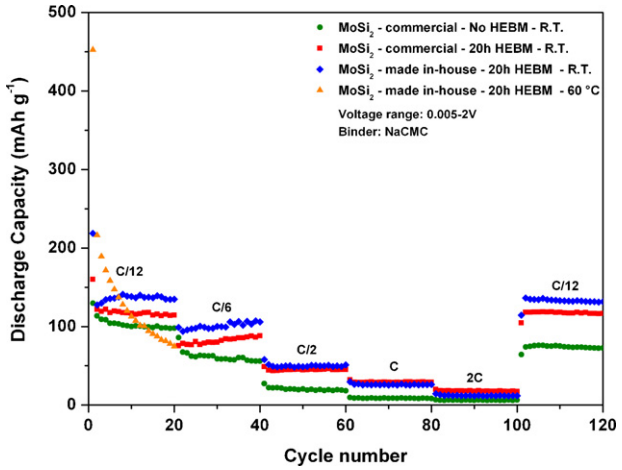

Fig. 6. Rate capability $MoSi_2$ anodes made from: as-received commercial powder cycled at R.T., commercial powder ball-milled for 20 h cycled at R.T., powder made in-house via 100 h of HEBM at R.T. and at 60 °C. Batteries were cycled between 5 mV and 2 V versus Li/Li^+ at C/12, C/6, C/2, C, 2C and back to C/12.

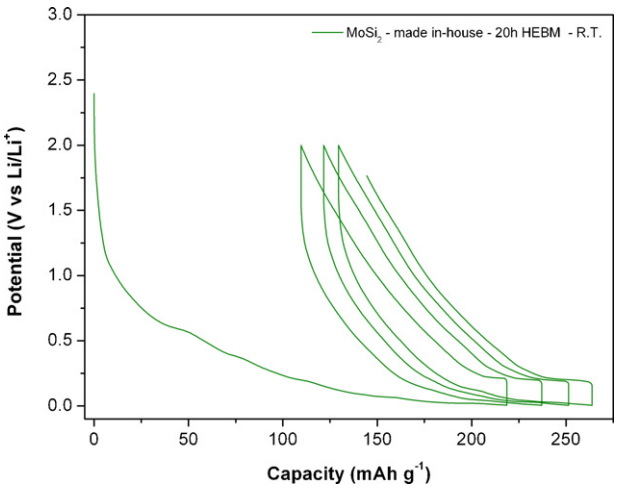

Fig. 7. Voltage profile of the first 4 cycles of $MoSi_2$ made in-house by 20 h of HEBM cycled at R.T. at C/12 between 5 mV and 2 V versus Li/Li^+.

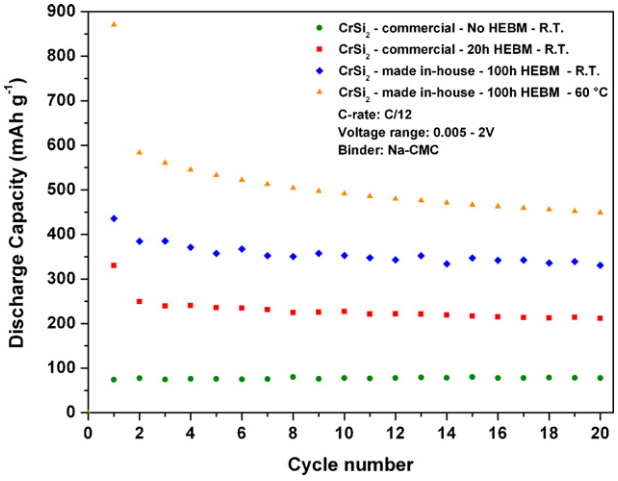

Fig. 8. Cycling behaviour of $CrSi_2$ anodes made from: as-received commercial powder cycled at R.T., commercial powder ball-milled for 20 h cycled at R.T., powder made in-house via 20 h of HEBM at R.T. and at 60 °C. Batteries were cycled between 5 mV and 2 V versus Li/Li^+ at C/12.

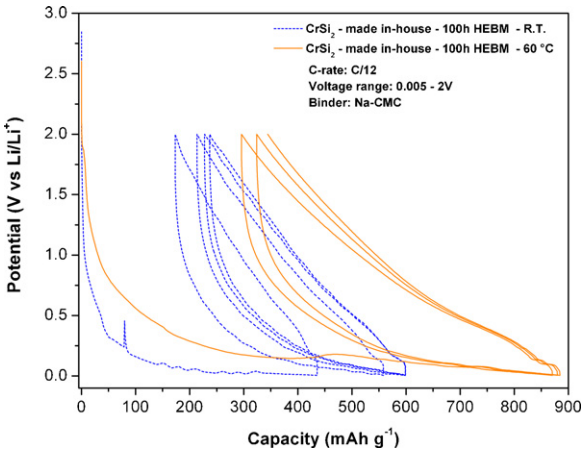

Fig. 10. Voltage profile of the first 4 cycles of $CrSi_2$ made in-house by 100 h of HEBM cycled at R.T. and 60 °C at C/12. Batteries were cycled between 5 mV and 2 V versus Li/Li^+.

reversible capacity of graphite for the same C-rate (330 mAh g^{-1}). The rate capability of the $CrSi_2$ powder prepared in-house is shown in Fig. 9. Capacities of 262, 167, 110, and 58 mAh g^{-1} were obtained at C/6, C/2, C, and 2C, respectively. When the battery was cycled back at C/12, the electrode recovered 94% of its previous capacity (at C/12). Similar to molybdenum, chromium does not form an alloy with lithium, and its addition to the binary silicon–lithium system produces four additional phases in the ternary phase diagram Cr–Si–Li: $CrSi_2$, CrSi, Cr_5Si_3, and Cr_3Si, which gave rise to three additional equilibria: $CrSi_2$–CrSi–$SiLi_{2.33}$, CrSi–Cr_5Si_3–$SiLi_{2.33}$, and Cr_5Si_3–Cr_3Si–$SiLi_{3.25}$ [14]. Eqs. (1)–(3) show the reactions corresponding to these equilibria:

$$3CrSi_2 + 7Li^+ + 7e^- \leftrightarrow 3CrSi + 3SiLi_{2.33} \quad (3)$$

$$15CrSi + 14Li^+ + 14e^- \leftrightarrow 3Cr_5Si_3 + 6SiLi_{2.33} \quad (4)$$

$$3Cr_5Si_3 + 13Li^+ + 13e^- \leftrightarrow 5Cr_3Si + 4SiLi_{3.25} \quad (5)$$

We observed that chromium silicide powders showed better performance than the molybdenum silicide powders. Contrary to $MoSi_2$, $CrSi_2$ is not a conductor but a p-type semi conductor with a band gap ranging from 0.3 to 0.84 eV [25] which results in lower electrical conductivity. According to Anani and Huggins study performed at 400 °C, it is mostly probable that lithium diffusion in $CrSi_2$ is quite low at R.T. [17]. So, in order to improve the lithium diffusion, a half-cell made of chromium silicide prepared in house by 100 h of HEBM was cycled at 60 °C. After 20 cycles at C/12, this electrode showed a capacity of 446 mAh g^{-1}, which is higher than the capacity obtained at R.T. The rate capability illustrated by Fig. 9, gave the following performance: 382, 315, 263, and 191 mAh g^{-1} at C/6, C/2, C, and 2C, respectively. When cycled back at C/12, the battery provided 360 mAh g^{-1} which represents about 81% of capacity recovery. However, a recovery of 94% was obtained when the battery was cycled at R.T., which means that the performance of the battery degrades faster when cycled at 60 °C. As for $MoSi_2$, this is most probably due to the formation of a thicker SEI that builds up with cycling at higher temperature, or due to the increased degree of $Li_{15}Si_4$ crystallization at 60 °C as opposed to amorphous $Li_{15}Si_4$, as reported by Fleischauer et al. [24].

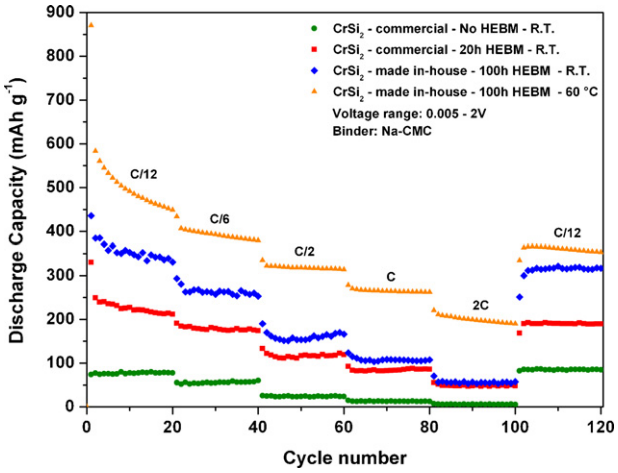

Fig. 9. Rate capability $CrSi_2$ anodes made from: as-received commercial powder cycled at R.T., commercial powder ball-milled for 20 h cycled at R.T., powder made in-house via 100 h of HEBM at R.T. and at 60 °C. Batteries were cycled between 5 mV and 2 V versus Li/Li^+ at C/12, C/6, C/2, C, 2C and back to C/12.

Fig. 10 shows the voltage profile of chromium silicide powder prepared in-house after 100 h of HEBM of Si and Cr powders. These batteries were cycled at R.T. or 60 °C at C/12 between 0.005 V and 2 V versus Li/Li^+. The general voltage profile is quite similar to what was observed for $MoSi_2$. The battery cycled at R.T. shows a shoulder at about 0.5 V that could be related to the formation of the SEI, whereas the same shoulder appears at about 1.8 V for the battery cycled at 60 °C. The potential then reached a plateau at about 0.04 V at R.T. and 0.17 V at 60 °C. These plateaus correspond to the formation of chromium-rich silicides and the formation of silicon–lithium alloys such as $SiLi_{3.25}$ and $SiLi_{2.33}$, according to equilibriums (3)–(5). Weydanz et al. observed the onset of the lithiation at slightly lower voltage of 300 mV for the Li–Cr–Si system [17]. The battery cycled at R.T. showed a first discharge capacity of 435 mAh g^{-1}, which represents 93% of the theoretical capacity. A first irreversible capacity of about 50 mAh g^{-1} (12% of the first discharge capacity) was measured. The same material cycled at 60 °C showed a higher first discharge capacity of 870 mAh g^{-1}, which is 85% higher than the theoretical capacity that we calculated for this powder. So it is probable that the extra capacity obtained at 60 °C corresponds to the formation of a thicker SEI on the surface of the $CrSi_2$ particles that consumes a large amount of charge. This high capacity came along with a high first irreversible capacity of 285 mAh g^{-1} (33% of the first discharge capacity). The delithiation of chromium silicide occurs as a slope, almost a straight line between 0.005 V and 2 V for both cycling temperatures. As previously mentioned, a larger irreversible capacity was observed for the battery discharged at 60 °C.

4. Conclusions

In this study we reported the investigation of molybdenum silicide and chromium silicide as anode materials for Li-ion batteries. The in-house prepared powders show better performance than the ball-milled commercial $MoSi_2$ and $CrSi_2$ powders. A HEBM time of 20 h was necessary for the appearance of the $MoSi_2$ crystalline phase whereas a longer time of 100 h was necessary for the formation of the $CrSi_2$ crystalline phase. Chromium silicide powders showed better performance than molybdenum silicide powders; more specifically the in-house prepared chromium silicide powder provided a capacity of 340 mAh g^{-1} at C/12. Higher cycling temperature showed a rapid decade of the capacity due to the degradation of the electrode.

Acknowledgment

This work was supported by Natural Resources Canada's Office of Energy Research and Development.

References

[1] G.-A. Nazri, G. Pistoia, Lithium Batteries: Science and Technology, Kluwer Academic Publisher, Boston, Dordrecht, New York, London, 2004.
[2] D. Larcher, S. Beattie, M. Morcrette, K. Edstrom, J.-C. Jumas, J.-M. Tarascon, J. Mater. Chem. 17 (2007) 3759–3772.
[3] J. Li, R.B. Lewis, J.R. Dahn, Electrochem. Solid-State Lett. 10 (2007) A17–A20.
[4] U. Kasavajjula, C. Wang, A.J. Appleby, J. Power Sources 163 (2007) 1003–1039.
[5] P.B. Balbuena, Y. Wang, Lithium-Ion Batteries: Solid-Electrolyte Interphase, Imperial College Press, London, 2004.
[6] A. Anani, R.A. Huggins, J. Power Sources 38 (1992) 363–372.
[7] J. Santos-Peña, T. Brousse, D. Schleich, Ionics 6 (2000) 133–138.
[8] H. Kim, J. Choi, H.-J. Sohn, T. Kang, J. Electrochem. Soc. 146 (1999) 4401–4405.
[9] M.D. Fleischauer, J.M. Topple, J.R. Dahn, Electrochem. Solid-State Lett. 8 (2005) A137–A140.
[10] E. Ma, J. Pagán, G. Cranford, M. Atzmon, J. Mater. Res. 8 (1993) 1836–1844.
[11] H.-Y. Lee, S.-M. Lee, J. Power Sources 112 (2002) 649–654.
[12] Y.-N. Zhou, W.-J. Li, H.-J. Chen, C. Liu, L. Zhang, Z. Fu, Electrochem. Commun. 13 (2011) 546–549.
[13] H. Wang, J.-C. Wu, Y. Shen, G. Li, Z. Zhang, G. Xing, D. Guo, D. Wang, Z. Dong, T. Wu, J. Am. Chem. Soc. 132 (2010) 15875–15877.
[14] A. Anani, R.A. Huggins, J. Power Sources 38 (1992) 351–362.
[15] C.-M. Park, J.-H. Kim, H. Kim, H.-J. Sohn, Chem. Soc. Rev. 39 (2010) 3115–3141.
[16] T. Moriga, K. Watanabe, D. Tsuji, S. Massaki, I. Nakabayashi, J. Solid State Chem. 153 (2000) 386–390.
[17] W.J. Weydanz, M. Wohlfahrt-Mehrens, R.A. Huggins, J. Power Sources 81–82 (1999) 237–242.
[18] H. Rietveld, Acta Crystallogr. 22 (1967) 151–152.
[19] BrukerAXS, DIFFRACPlus TOPAS: TOPAS 4.2 User Manual, Karlsruhe, Germany, Bruker-AXS GmbH, 2008.
[20] R.W. Cheary, A. Coelho, J. Appl. Crystallogr. 25 (1992) 109–121.
[21] R.S. Treptow, J. Chem. Educ. 80 (2003) 1015–1020.
[22] S. Köbel, J. Plüschke, U. Vogt, T.J. Graule, Ceram. Int. 30 (2004) 2105–2110.
[23] Z. Guo, G. Blugan, T. Graule, M. Reece, J. Kuebler, J. Eur. Ceram. Soc. 27 (2007) 2153–2161.
[24] M.D. Fleischauer, R. Mar, J.R. Dahn, J. Electrochem. Soc. 154 (2007) A151–A155.
[25] H.N. Zhu, K.Y. Gao, B.X. Liu, J. Phys. D: Appl. Phys. 33 (2000) L49.